

IMPROVEMENT OF THE ACOUSTO-ULTRASONIC METHOD USING MODEL ANCHOR BASES WITH CONTROLLED DEFECTS

R. JOHANNES*, N. GODIN[†] AND L. GAILLET*

* University Gustave Eiffel

All. des Ponts et Chaussées 44340 Bouguenais

e-mail: raphael.johannes@univ-eiffel.fr, laurent.gaillet@univ-eiffel.fr

[†]INSA de Lyon, Univ. Lyon, MATEIS UMR 5510

7, Avenue Jean Capelle 69621 Villeurbanne

e-mail: nathalie.godin@insa-lyon.fr

Key words: Damage, Controle, Cable, Acousto-Ultrasound

Abstract. Cables in engineering structures are essential to the integrity of the structure. However, they are subject to damage in specific areas, particularly at the cable entry into the anchor base. Currently, there are no non-destructive testing techniques available for examining this area. The aim of this work is to study the feasibility of defect detection using acousto-ultrasounds. These combine ultrasound and acoustic emission. Tests on suspension bridges have shown that the technique is sensitive to the state of health of the bases. However, in order to quantify the nature of the defect and determine its severity, a study is being carried out on "model" anchor bases, manufactured on a real scale: two bases without defects and four reproducing defects observed during inspections of bridges (mechanical failure and corrosion of the cable's external wires, presence of a void in the fusible material). The first step was to optimise the choice of sensors for transmission and reception and their position. Then, a detailed analysis of the descriptors extracted from the signals is carried out to determine the presence of a defect and assess its severity.

1 INTRODUCTION

The multi-layer cables used in suspension and cable-stayed bridges play a crucial role in the stability and safety of these structures [1]. Regular inspection and maintenance are essential to ensure the safety of the bridge. Non-destructive testing techniques such as magnetic particle inspection, ultrasound and acoustic emission are used to monitor the accessible parts of the cables. However, the ends of the cables, embedded in anchor bases and sealed with a fusible material such as zinc, remain inaccessible to conventional methods. The area where the cable enters the socket is particularly vulnerable. It suffers damage from water run-off, leading to stagnation that encourages wire corrosion. In addition, friction between the wires in this highly stressed area can cause them to break. Current research is aimed at developing a method for assessing the condition of cables inside anchor bases. In situ inspections have demonstrated the potential of a technique capable of comparing the condition of cables in these critical areas, while highlighting areas for improvement. The manufacture of full-scale anchor bases with controlled defects will enable this method to be refined, in particular by perfecting the acousto-ultrasound technique for a more reliable assessment (Figure 1).

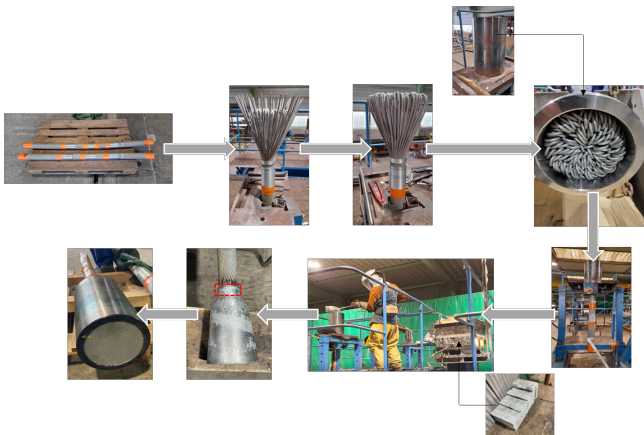


Figure 1: Model anchor manufacturing process.

2 METHOD

The method used to auscultate anchor is based on acousto-ultrasound (AU), a technique that combines acoustic and ultrasound emissions. It involves generating an ultrasound signal using an transducer placed at the bottom of the anchor (see Figure 2 and 3). The elastic wave emitted passes through the base, which is made of a heterogeneous material (zinc alloy as a fusible material and low-alloy steel cables). The wave is then picked up by four sensors positioned around the cable (Figure 2). These sensors record the waves that have passed through the end of the cable. Once intercepted, the elastic waves are converted into electrical signals by the piezoelectric sensors. These signals are amplified using preamplifiers (40 dB gain) before being transmitted to the acquisition system dedicated to acoustic emission (EA), based on an Express8 chain.

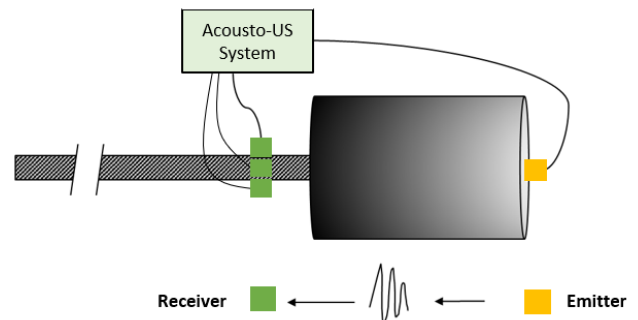


Figure 2: Diagram of an instrumented anchor base [2].



Figure 3: Instrumentation of a model anchor base.

Initially, R15 piezoelectric sensors were used, with 4 receiving sensors and 1 transmitting sensor (emission frequency: 150 kHz (Figure 4a)). In a second phase, micro 80 type sensors were used, with 1 transmitting sensor and 3 receiving sensors (emission frequency: 320 kHz (Figure 4b)). The diameter of the surface of the micro 80 sensors is smaller ($\varnothing 9\text{mm}$) than that of the R15 ($\varnothing 18\text{mm}$), allowing the sensor to be positioned on the wires, but leaving less space between two wires (wire $\varnothing 5.6\text{mm}$). When the reception sensors are positioned around the cable, an auto sensor test (AST), in which each sensor receives and extends a wave generated by the system, it is used to observe the coupling between the sensors and the cable.

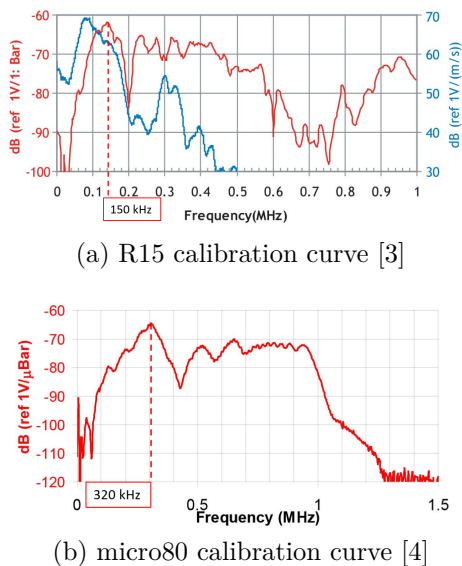


Figure 4: calibration curves for sensor sensitivity at reception

During tests, the ARB card's transmission parameters was a square wave signal at a frequency of 150 kHz for R15 sensor and 320kHz for micro80 sensor, emitted every two seconds over a period of one minute. A power sweep, ranging from 1 to 10 V with ARB1410 chain (Mistras group) (Figure 5), was performed to assess the impact of the emission intensity. This scan revealed no significant difference in the qualitative results, apart

from an increase in the descriptor values, consistent with the increase in wave power.

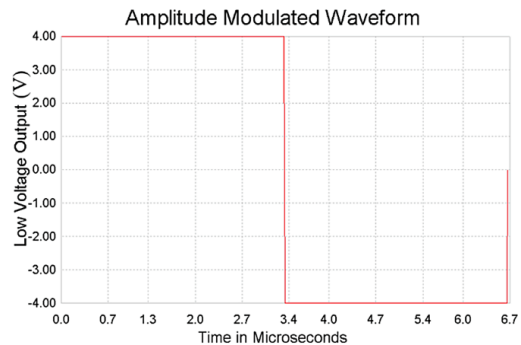


Figure 5: Square wave signal emitted by the ARB1410 chain. [5]

The Acoustic Emission (AE) chain (PCI Express8 Mistras group) is used to record the signals collected. The main descriptors of the common signal are listed in table 1. With regard to the reception of waves after they have passed through the base, the acquisition threshold for signal recording is set at 35 dB. Specific parameters such as PDT (Peak Definition Time)= $300\mu\text{s}$, HLT (Hit Lockout Time)= $600\mu\text{s}$ and HDT (Hit Definition Time)= $1000\mu\text{s}$ are adjusted to take account of the reduced transmission properties of the material under study.

Table 1: Time and frequency descriptors used to process signals [6]

ID	Feature	Unit
Time Features		
R1	Amplitude	dB
R2	Duration	μs
R3	Energy	$\mu\text{V}\cdot\text{s}$
R5	Rise time	μs
Frequency Features		
R8	Partial Power 1 ([0; 100] kHz)	%
R9	Partial Power 2 ([100; 200] kHz)	%
R10	Partial Power 3 ([200; 250] kHz)	%
R11	Partial Power 4 ([250; 400] kHz)	%
R12	Frequency centroid	kHz
R13	Peak frequency	kHz

3 MODEL ANCHOR BASES

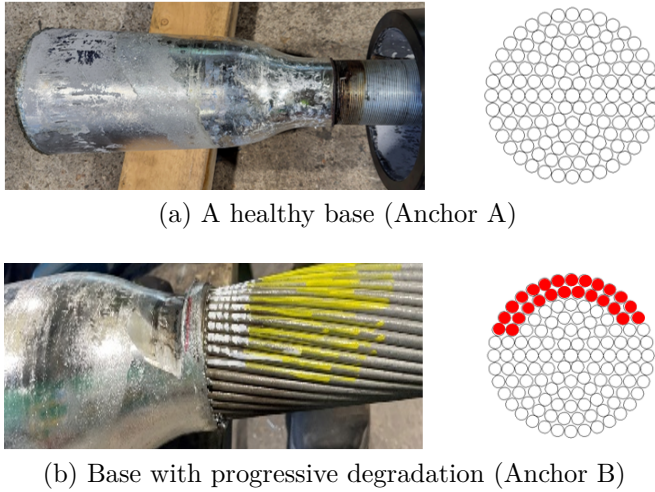


Figure 6: Model anchor bases (number of wires cut in red)

The production of model-scale bases provides an essential reference base for in-depth signal transmission analysis. Some of the degradations simulated on these models are inspired by those observed on cables extracted from their bases. The most common degradations include a lack of fusible material, sharp wire breaks and corrosion on the outer layers of the cables. The anchor A will be used as a reference during the tests, as they show no degradation either on the cable or inside the base (Figure 6a). On the other hand, the anchor B has been designed with progressive degradation of the cable to simulate the initiation and propagation phases of corrosion (Size: length 70mm/ width: 20mm/ depth: 17mm), (see Figure 6b). Initially, the degraded anchor base will be analysed. The aim is to identify variations in the signals picked up between the sensors as a function of their position on the cable. Secondly, a comparison will be made between a healthy anchor (example: Anchor A) and a degraded anchor base (Anchor B). The aim is to assess the technique's ability to differentiate between a healthy bases and with defects. This analysis will make it possible to identify the most relevant descriptors for characterising degra-

dations, whether they be wire breaks, corrosion or a lack of fusible material. The results obtained will be crucial in validating the effectiveness of the method and refining the detection parameters.

By comparing the signals received from the sensors on the same anchor base, the aim is also to locate the area of cable damage inside the base, using the sensors positioned around the cable (Figures 7 and 8).

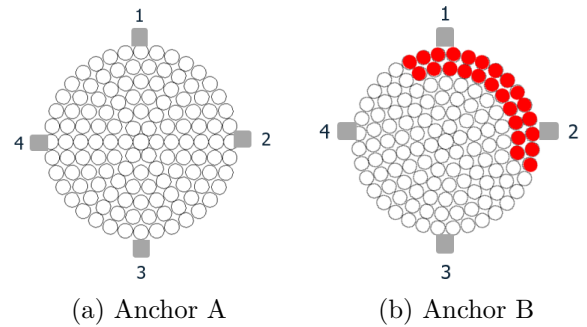


Figure 7: Positioning the R15 sensors on the various anchor bases

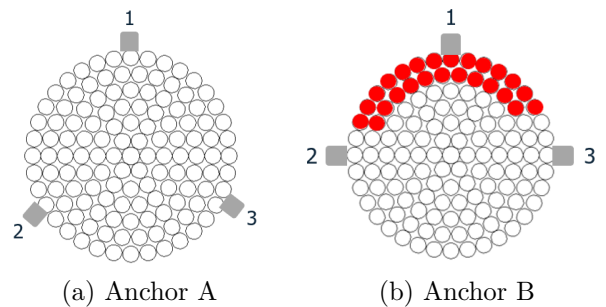


Figure 8: Positioning the micro80 sensors on the various anchor bases

4 RESULTS

The parameters used during the tests are detailed in the method section. The descriptors will be displayed with a power of 5 V, as the increase in data when the power is increased has no effect on the interpretation.

4.1 Reference data obtained with anchor A (R15 and micro80 sensor)

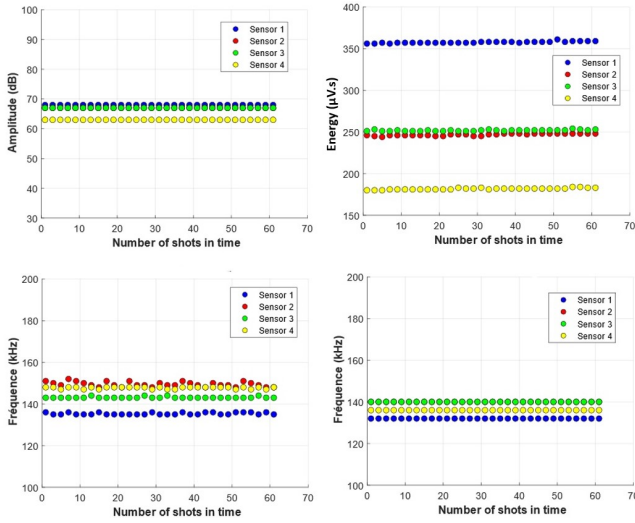


Figure 9: Amplitude (dB), energy ($\mu\text{V.s}$), frequency centroid (kHz) and peak frequency (kHz) as function of the number of shots over time for the R15 sensor on anchor A (healthy).

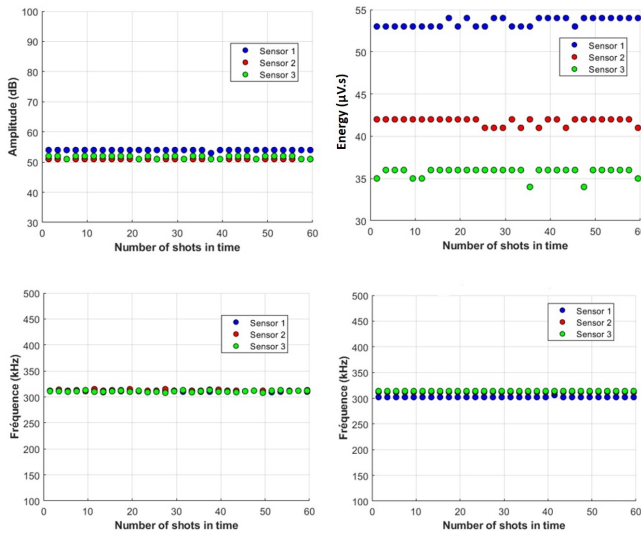
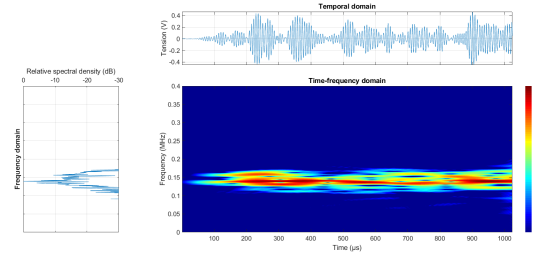


Figure 10: Amplitude (dB), energy ($\mu\text{V.s}$), frequency centroid (kHz) and peak frequency (kHz) as function of the number of shots over time for the micro80 sensor on anchor A.

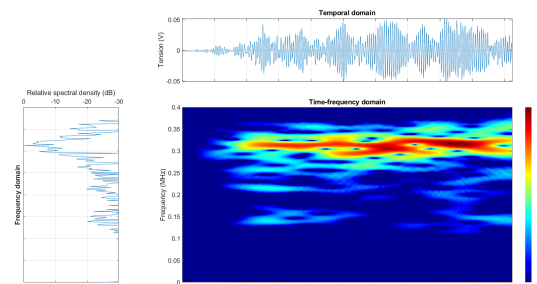
On the healthy base (Anchor A) (Figure 6a), all the sensors were positioned on healthy areas (Figure 9). There was little variation between the sensors for the signal

descriptors (amplitude, frequency centroid and peak frequency). In contrast to the other descriptors (Figure 9), there is a strong dispersion between R15 sensors for energy with a factor of $176 \mu\text{V.s}$ between the minimum and the maximum with the micro80 sensors this factor is much lower $18 \mu\text{V.s}$ (Figure 10). This could be due to a coupling problem between the sensor and the cable, or to wave dispersion due to the complex propagation environment.

The micro80 sensors are positioned on healthy parts (Figure 8a). There were few differences in the amplitude, frequency centroid and frequency peak descriptors (Figure 10). As far as energy is concerned, there was a slight dispersion between the sensors, a phenomenon also noted during the AST. The R15 and micro80 sensors showed that the frequency descriptors are close for all the sensors.



(a) Time-frequency analysis for an R15 sensor on anchor A.



(b) Time-frequency analysis for an Micro80 sensor on anchor A.

Figure 11: Time-frequency analysis for sensors on anchor A.

The signals recovered by the R15 and micro80 sensors on a healthy anchor base were

observed using time-frequency analysis (Figure 11). The resonance frequencies were found for both sensors. For the R15 sensor the peak is at 150 kHz (Figure 11a). For the micro80 sensor the peak is at 320 kHz (Figure 11b), we also observe smaller signals before the peak, which is explained by the wider band around its resonance frequency (Figure 4b). The time-frequency analysis shows undisturbed signals for both sensors for anchor A.

4.2 Comparison of the anchor B with anchor A (Reference) (R15 and micro80 sensor)

On the base with a progressive degradation (Anchor B) (Figure 6b), R15 sensors 1 and 2 are positioned in the extension of the cut wires (Figure 7b), while sensors 3 and 4 are placed on healthy areas of the cable. In terms of signal amplitude (Figure 12), sensors 1 and 2 show a less efficient response compared with sensors 3 and 4. In terms of energy, sensors 1, 2 and 4 show low values compared with sensor 3. If we compare with the range of signals obtained on the healthy anchor (anchor A) (63 to 68dB for the amplitude and from 180 to 356 $\mu\text{V}\cdot\text{s}$ for energy (blue zone)) sensors 1 and 2 are weaker on both descriptors (Figure 12). When we compare sensors 3 and 4 which are on healthy areas of anchor B the results obtained are close to the signals obtained for anchor A. Sensor 4 is weaker than sensor 3 on energy, it is closer to the cut wires. The micro80 sensor 1 is positioned in the extension of the cut wires, while sensors 2 and 3 are placed on healthy parts (Figure 8b). The amplitude and energy descriptors show that the signal received by sensor 1 (48 dB and 27 $\mu\text{V}\cdot\text{s}$) is weaker than those obtained by sensors 2 (58 dB and 57 $\mu\text{V}\cdot\text{s}$) and 3 (51 dB and 46 $\mu\text{V}\cdot\text{s}$) (Figure 13). When we compare the signals obtained from anchor B with those from anchor A (blue zone 51 to 54dB for amplitude and 35 to 53 $\mu\text{V}\cdot\text{s}$ for energy), sensor 1, which is on the extension of the cut wires, has a sig-

nal with a lower amplitude but similar energy to the signals obtained from the healthy anchor. This difference in energy observed may be due to reflection within the propagation medium.

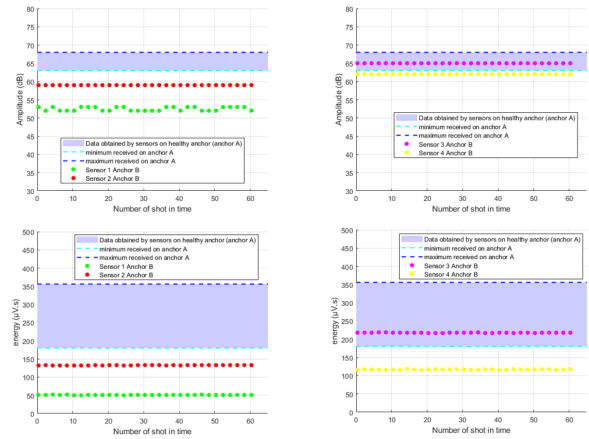


Figure 12: Comparison of the signals obtained with the R15 sensors on anchor B with the signals obtained on anchor A (blue zone) in amplitude (dB) and energy ($\mu\text{V}\cdot\text{s}$).

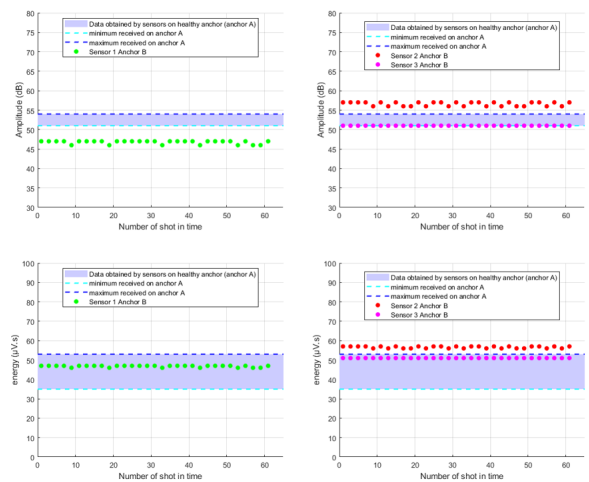


Figure 13: Comparison of the signals obtained with the Micro80 sensors on anchor B with the signals obtained on anchor A (blue zone) in amplitude (dB) and energy ($\mu\text{V}\cdot\text{s}$).

The frequency descriptors of the sensors in the areas with and without defects show little difference, but to observe greater dispersions, it would be interesting to extract other frequency descriptors or to observe the

signals obtained using a time-frequency analysis.

Determining the fracture zones on the same base according to the positioning of the sensors is proving promising. The tests carried out showed a reduction in amplitude and energy when the sensors were positioned over an area with defects. Similar observations were reported during in situ campaigns on the anchors of a suspension bridge [7]. With R15 transducers, a decrease in amplitude was observed for transducers positioned on the extension of cut wires.

Thanks to the results obtained for the two bases, it is possible to compare them with each other. The sensors placed on the anchor A recorded a wave close to or slightly higher than that of the sensors placed on healthy parts of the Anchor B. On the other hand, for the sensors placed on the extension of the defects, the amplitudes are lower than those recorded by the sensors located on a healthy base. Energy showed good results with the R15 sensors, but less significant results with the micro80 sensors.

5 CONCLUSIONS

The first tests of the anchor bases, healthy models with controlled defects, showed consistency between the reduction in the amplitude and energy of the signal received by the sensors and their positioning on the extension of the cut wires. A comparison of the tests carried out with the Micro80 and R15 sensors revealed that the Micro80 sensors had a lower amplitude and energy in reception. This can be attributed to the smaller surface area of the Micro80 sensors, but also to their higher resonance frequency (320 kHz compared with 150 kHz), which attenuates the signal more when the propagation distance is large. However, the Micro80 sensors showed reliable responses in the tests, with little variation between healthy areas and significant signal attenuation in areas with

defects on the same anchor base, compared with the R15 sensors, which proved more dispersive. The next stage of these tests will involve testing broadband sensors and combining different types of sensor to improve the detection methodology. The choice of coupling will be made once the most suitable sensors have been selected. Repeatability remains a key issue for the NDT inspections of anchors. It is necessary to continue to carry out measurements collecting additional data to feed a database with a view to applying supervised classification techniques.

REFERENCES

- [1] Niels J. Gimsing and Christos T. Georgakis. *Cable Supported Bridges: Concept and Design*. 1st ed. Wiley, Dec. 23, 2011.
- [2] M. Kharrat and L. Gaillet. “Non-Destructive Evaluation of Anchorage Zones by Ultrasonics Techniques”. In: *Ultrasonics* 61 (Aug. 2015), pp. 52–61.
- [3] Physical Acoustics Corporation and Mistras. R15 Sensor. 2011.
- [4] Physical Acoustics Corporation and Mistras. Micro80 Sensor. 2011.
- [5] Cheikh A. T. Sarr et al. “Nondestructive Evaluation of FRP-reinforced Structures Bonded Joints Using Acousto-Ultrasonic: Towards Diagnostic of Damage State”. In: *Construction and Building Materials* 313 (Dec. 27, 2021), p. 125499.
- [6] N. Morizet et al. “Classification of Acoustic Emission Signals Using Wavelets and Random Forests : Application to Localized Corrosion”. In: *Mechanical Systems and Signal Processing* 70–71 (Mar. 2016), pp. 1026–1037.
- [7] R Johannes, N Godin, and L Gaillet. “Application of the Acousto-ultrasonics Technique to Bridge Cables in Their Anchorages.” In: *e-Journal of Nondestructive Testing* 29.10 (Oct. 2024).